Nontraumatic Implant Explantation: A Biomechanical and Biological Analysis in Sheep Tibia

Eduardo Anitua, MD, DDS, PhD[1,2]*
Alia Murias-Freijo, DDS[1]
Laura Piñas, DDS[1]
Ricardo Tejero, MEng, PhD[2]
Roberto Prado, MSc[2]
Gorka Orive, PhD[2]

Preclinical research in a sheep tibia model has been conducted to evaluate the underlying mechanisms of the nontraumatic implant explantation of failed implants, which allow placing a new one in the bone bed. Twelve dental implants were placed in sheep diaphysis tibia and once osseointegrated they were explanted using a nontraumatic implant explantation approach. Implant osseointegration and explantation were monitored by means of frequency resonance, removal torque, and angle of rotation measurement. The host bone bed and the explanted implant surface were analyzed by conventional microscopy and scanning electron microscope. Results show that osseointegration was broken with an angular displacement of less than 20°. In this situation the implant returns to implant stability quotient values in the same range of their primary stability. Moreover, the explantation technique causes minimal damage to the surrounding bone structure and cellularity. This nontraumatic approach allows the straightforward replacement of failed implants and emerges as a promising strategy to resolve clinically challenging situations.

Key Words: implant removal, explantation, animal model, osseointegration, nontraumatic

INTRODUCTION

In the few last decades, oral implantology has achieved high rates of success in implant placement, with survival rates greater than 90%,[1,2] and, in some cases, even reaching 99%.[3] The success of implant-based restorations relies on the achievement of suitable osseointegration. Branemark et al first described osseointegration as the structural and functional connection between vital bone and the surface of a load-bearing implant.[4,5]

Despite the high success rates reported, a number of dental implants still fail in daily practice. Implant failure may be due to several reasons including peri-implantitis, excessive occlusal load, incorrect placement, suboptimal implant design, and improper prosthetic constructions.[6–9] When no palliative treatment can be applied, the failing implant has to be removed and replaced by a new implant, using trephination as the conventional removal technique.[10] Together with the implant, trephination removes a cylindrical corona around the implant, creating a large cylindrical bone defect. Other approaches available for implant removal involve the use of piezoelectric devices, counter-torque ratchets, high-speed burs, elevators, thermal- or laser-assisted explantators, edentulous ridge expansion, forceps, or procedures that combine some of the aforementioned methods.[10–15]

The choice of the explantation method to be used is critical, because it may significantly affect subsequent retreatment. The size of the bone defect, the possible bone overheating, the damage to adjacent tissues, and the presence of titanium particles from the removed implant[14] are critical factors that may influence the healing time, the number of surgeries needed, and the time of final functional restoration with important implications in the costs and well-being of the patient.

Recently, a method for noninvasive explantation has been developed, which allows preserving the maximum bone bed.[16] This nontraumatic countertorque explantation system allows placing a new implant of the same or greater diameter than the explanted one in the same surgical approach. Its clinical use has been previously described in a series of 42 patients and 91 implants of different brands and dimensions, showing that the technique is predictable and safe to remove implants both from the maxilla and the mandible.[16]

In this study, we have used an animal model to understand the biomechanical and biological mechanisms involved in this process. To that end, we first inserted dental implants in sheep tibia and once osseointegrated, implants were explanted using the nontraumatic implant explantation approach. Implant osseointegration and explantation[17] were monitored by means of frequency resonance, removal torque, and angle of rotation measurement. Furthermore, a complete histological analysis of the remaining bone bed and implant surface examination using scanning electron microscopy were carried out.

[1] Private practice in implantology and oral rehabilitation, Vitoria, Spain.
[2] Biotechnology Institute (BTI), Vitoria, Spain.
* *Corresponding author,* e-mail: eduardoanitua@eduardoanitua.com
DOI: 10.1563/aaid-joi-D-14-00193

Material and Methods

Titanium implant preparation and surface characterization

Fifteen Ø 4.0 mm × 6.5 mm BTI Interna implants (reference IIPU4065, BTI Biotechnology Institute S.L., Vitoria, Spain) were surface modified according to the manufacturer's proprietary method. The surface roughness of 3 implants was measured by optical profilometry (3D Sensofar Plμ, Terrasa, Spain). A Gaussian filter of 20 × 20 μm was used to separate roughness from waviness. The main roughness values obtained were Sa = 0.75 ± 0.06 μm, Sq = 1.01 ± 0.10 μm, Sdr = 86.51 ± 10.05%. After implant cleaning and conditioning, the surface chemistry consisted primarily of titanium dioxide with less than 20% carbon, as confirmed by X-ray photoelectron spectroscopy (XPS, SPECS SAGE HR 100, Berlin, Germany). Implants were packaged individually and sterilized with beta irradiation at 25 kGy before use.

Animal model and surgical procedures

All surgical procedures were performed under sterile conditions in a veterinary operating room. Twelve implants were placed monocortically in the medial aspect of the diaphysis of the sheep tibia (6 in each leg). After sedation, an intramuscular injection of ketamine (10 mg/kg) to be subsequently conducted spinal anesthesia with 3 mL of bupivacaine (0.5%) was used. During surgery, antibiotic prophylaxis (1 g intravenous cefonicid) and analgesic (intravenous fentanyl) were administered. After skin and fasciae dissection, the tibia was exposed. A previously described sequential drilling was used.[18] A home-made titanium template with 6 holes was used to guide the initial drill and preserve a constant implant separation. The template was fixed with 2 mini screws to the tibia and was removed for the subsequent drilling operations (Figure 1a) of growing diameters (3.0, 3.25, 3.5, and 3.8 mm, Figure 1b). The implant sites were finally cleaned with saline solution to remove bone debris. The implants were placed with a uniform torque of 50 Ncm (Figure 1c), until all 6 implants were perfectly placed in each tibia (Figure 1d). The implant primary stability was measured by resonance frequency analysis (RFA; Figure 1e). Finally, the surgical wound was closed in layers. The periosteum was first sutured taking care not to damage it (Figure 1f) and the skin was closed with staples.

A postoperative antibiotic was administered for 5 days (cefonicid, 1 g). All sheep were inspected daily and analgesics and anti-inflammatory drugs were administered if necessary. The staples were removed 10 days after surgery.

Both tibias were dissected and extracted 22 weeks later. Analysis procedures were performed on the same day of the extraction. Tibiae were wrapped in saline-soaked gauze to prevent dehydration and were kept at 4 °C until use. Two intact implants were used to confirm the osseointegration by histological analysis, while the other 10 were employed in the RFA and in the measurements of angle and torque explantation studies.

All procedures were performed following the guidelines established by the ISO 10993-6:2007 (Biological evaluation of medical devices, Part 6: Tests for local effects after implantation), specifically Annex D, corresponding to test methods for implantation in bone. Animal handling and surgical procedures were carried out according to the directive of the European Parliament and Council of the European Communities (2010/63/UE) and the Spanish legislation (RD 1201/2005 and Law 32/2007). The local ethics committee approved the protocol of this study.

Radiographic follow-up

A high resolution (> 20 lp/mm) digital radiography system (Kodak RVG 6100, Eastman Kodak Company, Rochester, NY) was used to follow the progress of implant osseointegration. Craniocaudal radiographs were taken immediately postsurgery, every 4 weeks until sheep sacrifice, and prior to explantation. Three implants were observed in each radiographic image.

Bone-implant histological characterization (osseointegration evaluation)

One intact implant with the surrounding bone per tibia was used for histological evaluation. Implants and surrounding tissue were fixed in 4% buffered formalin solution for at least 24 hours, dehydrated in graded series of ethanol solutions ranging from 70% to 100%, and embedded in a light-curing acrylic resin (Technovit 7200 VLC, Heraeus Kulzer, Wehrheim, Germany) according to the manufacturer's instructions. After polymerization, the blocks were cut to a thickness of 300 μm and polished to their final thickness. Two nondecalcified 20 μm-thick sections of the implants following their longitudinal axis were obtained using a diamond saw and a grinding/polishing machine (Exakt Technologies, Oklahoma City, Okla). Sections were stained with Harris hematoxylin plus Wheatley's trichrome stain for optical microscopy examination with a Leica DMLB light microscope (Leica Microsystems, Wetzlar, Germany) coupled to a Leica DFC300FX digital camera (Leica Microsystems).

Resonance frequency analysis for stability assessment of implants

Quantitative measurements of implant stability were achieved with the use of RFA (Osstell ISQ, Göteborg, Sweden), which provides an implant stability quotient (ISQ), which ranges from 1 to 100, where 1 is the lowest and 100 the highest degree of stability. Three measurements were performed on each implant: the first immediately after placement, the second 22 weeks after surgery and before explantation, and the third after explantation (osseointegration breakdown).

Removal torque and angle measurement

Tibiae were fixed with a multi-angle bench vise and 10 implants were measured (5 per tibia). Implant removal torque and rotation angle measurements were performed with a custom-made device consisting of the following components: (1) a tool connecting the implant to the torque wrench (INEXIM2, BTI Biotechnology Institute). This tool uses the torsional capacity of the internal connection of the implant to apply the extraction torque. (2) A torque wrench with strain gauges, comprising an explantation torque wrench from BTI (LLT200; BTI Biotechnology Institute) with one full bridge of 4 strain gauges in bending configuration (EA-06-125BZ-350, Vishay Precision Group—Micro-Measurements, Madrid, Spain). Strain gauges were installed in the outer surface of the tube of the wrench. (3)

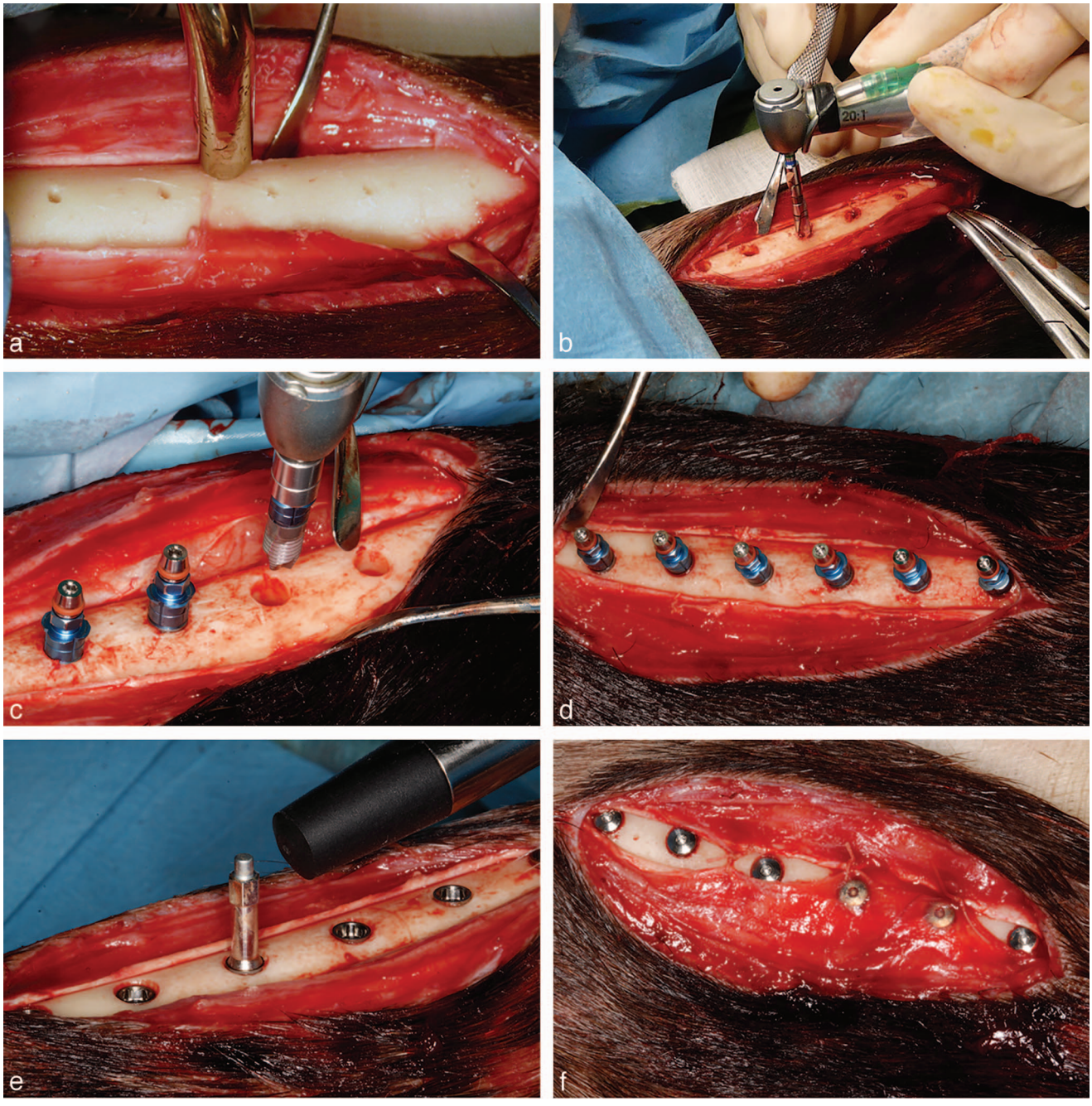

Figure 1. Implant surgery in sheep tibia. The holes made with the initial drill (a), guide the subsequent drilling sequence (b), and place the implants (c). Once the implants have been placed (d), primary stability is measured with Osstell ISQ (e). The surgical wound is closed in layers, starting with the periosteum (f).

An angle sensor encoder (AEDA-3300-TAT, Agilent Technologies, Santa Clara, Calif) with a resolution of 4096 points per turn (0.087°), and finally (4) a data recorder with 16 channels and 100 Khz 16 bit A/D converter (Somat e-DAQ Plus, HBM Inc. Marlborough, Mass). The data from the strain gauges and the encoder was recorded simultaneously during the process of explantation. This full assembly was previously calibrated with an electronic torque wrench (TSD 1500, Torqueleader, Bramley, Surrey, UK). The resolution achieved was 1 Ncm.

Explantation process was carried out similarly to the protocol used in clinical practice.[16] The removal torque was measured in real time and it was stopped when implant torque decreased. Data were converted to csv format and postprocessed with in-site software for signal treatment, compiled with C++ Builder 2010 (Embarcadero Technologies, San Francisco, Calif). The raw data obtained from each implant were processed with the Solver program within the Office Excel software (Microsoft, Redmond, Wash) using the smooth-

ing and fitting of a polynomial equation of 3 terms with variable exponents.

Implant surface characterization after explantation

The surface of the implants was studied with a scanning electron microscope (SEM; JEOL JSM-6490LV; Tokyo, Japan). Due to the presence of organic components on the surface after explantation, samples were fixed with 2.5% glutaraldehyde (Sigma-Aldrich, St Louis, Mo) solution in phosphate buffered saline (PBS, Sigma-Aldrich) for 8 hours. The samples were then dehydrated by sequential immersion in serial diluted solutions of 0%, 10%, 30%, 50%, 70%, 90%, and 100% v/v of ethanol in water. Dehydrated samples were then air-dried, coated with gold-palladium in a sample preparation chamber with sputtering system (Gatan Alto 1000E, Nuffield, UK) and examined by SEM. Images were taken at 10 kV acceleration voltage. Backscattered electron mode allows a better contrast between materials of different electronic density and thus, this scanning mode was used preferentially. The SEM-attached energy dispersive X-ray unit served to analyze the elemental composition of the surface remnants.

Bone defect characterization after explantation

After explantation, conventional microscopy and SEM were used for analysis of the remaining bone defects. First, the tibia was cut along its cross-axis between the bone defects. Then, each sample was cut in half with the same orientation. Thus, half of each bone defect was observed with each technique.

For SEM examination, the samples were rinsed with PBS, fixed with 2% glutaraldehyde in 0.1 M cacodylate buffer for 1 hour and washed 3 times in cacodylate–sucrose buffer (0.1 M cacodylate, 6.5% sucrose, pH 7.4). Then, the samples were postfixed with osmium tetroxide (1% OsO4 in 0.1 M cacodylate) for 1 hour and washed in 0.1 M cacodylate, and finally dehydrated through ascending alcohol concentrations. Next, the samples were subjected to critical point drying (Autosamdri 814, Tousimis, Rockville, Md) and sputter-coated with 5 nm of gold (E306A, Edwards, Crawley, West Sussex, UK) before examination in an electron microscope (S-4800, Hitachi, Chiyoda, Japan).

For optical microscopy the samples were fixed in formaldehyde (4%) at 4°C for at least 1 week, dehydrated in ascending concentrations of ethanol and embedded in a low-temperature acrylic resin (Technovit 9100 New, Heraeus-Kulzer) and processed according to a standard protocol for undecalcified bone samples.[19] Next, 5-μm-thick sections were cut, stained with May-Grünwald-Giemsa (MGG), and observed under microscopy (DMLB, Leica Microsystems) equipped with a digital camera (DFC300FX, Leica Microsystems).

Statistics

The normality of the ISQ values obtained was confirmed by the Kolmogorov–Smirnov test and prior to the repeated-measures ANOVA test of variance (SPSS 15.0, IBM, Chicago, Ill). *P*-values $<$ 0.05 were considered statistically significant. All values were expressed as mean $\pm$ *SD*.

Results

Animal model and osseointegration evaluation

All sheep tolerated the surgery and no relevant problems were observed. There were no signs of inflammation or infection. All implants were placed monocortically and were clinically immobile (Figure 2a). The radiographs taken during the osseointegration follow-up showed no evidence of implant failure (Figure 2b and c). The implants retrieved with the peri-implant osseous tissue confirmed the complete osseointegration (Figure 2d). Continuity was observed in osteons, and close contact was observed between the compact bone and the implant, without the presence of fibrous tissue (Figure 2e).

Implant stability values

The implant stability values (ISQ) obtained by resonance frequency analysis with Osstell are shown in Figure 3. At implant placement, the ISQ value was 80.8 $\pm$ 3.0, whereas 22 weeks later it increased to 88.2 $\pm$ 1.8 ($P < 0.005$). The ISQ value after osseointegration breakdown was 78.3 $\pm$ 4.9, similar to the value retrieved at the time of placement and inferior to those obtained at 22 weeks pre-explantation ($P < 0.005$).

Removal torque and implant rotation angle

The values of removal torque and rotation angle were obtained with the custom-made device as shown in Figure 4a. Nine explants were analyzed. Data from 1 explantation was lost due to technical reasons. In each removal test, the torque-angle curve was recorded and observed in real time.

The removal torque value accords to the maximum torque value recorded: 228 $\pm$ 18 Ncm. The corresponding angle was considered the extraction angle: 19 $\pm$ 3° (Figure 4b).

Fig. 4C shows the curves of extraction torque vs angle for the 9 implants tested. The curves can be subdivided in 3 main regions: (1) The linear region, where angle and torque values are low and the behavior of the implant within the host bone is still mainly elastic; (2) the breakdown region, where the torque reaches its maximum and the osseointegration is progressively lost until the complete detachment of the implant bone from the host bone due to the shear forces; and (3) the relaxation region, in which the torque decreases and the implant turns easily with smaller forces. In this area, only frictional forces between bone and implant are present.

Implant surface characterization after explantation

Scanning electron microscopy was used to analyze the surfaces of the implants retrieved from sheep tibia. The composition of the remaining components obtained after explantation was analyzed by EDX. Figure 5a shows the surface of an explanted implant in which the organic (darker) and inorganic (brighter) parts of bone can be observed. The explantation procedure allows the separation of the implant from the surrounding bone and only bone remnants can be detected at the apical sites.

EDX mapping at the implant neck confirmed the presence of cells. Although the techniques used did not help to determine the phenotype of the cells, their morphology

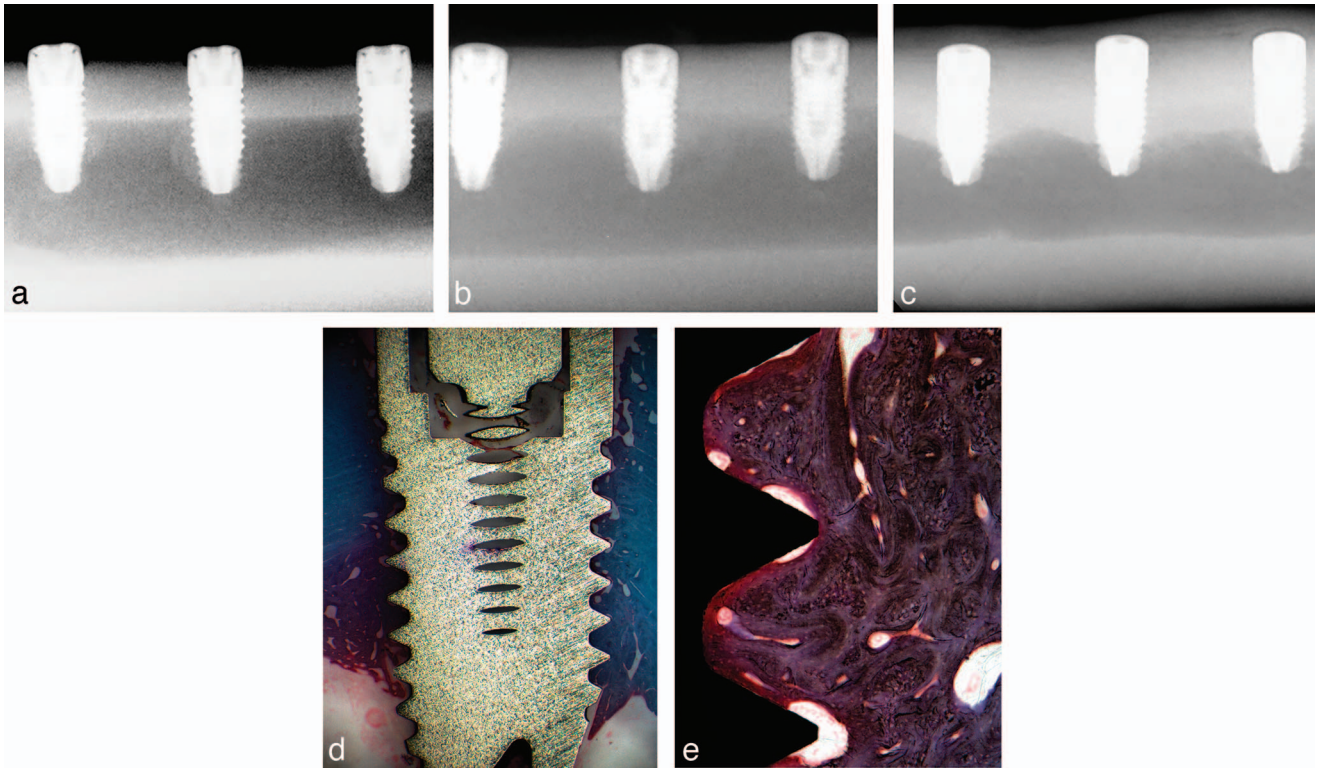

Figure 2. Implant osseointegration: radiographic follow up (a–c) and histological images (d–e). Examples of craniocaudal radiographs taken after placement of the implants (a), four weeks after surgery (b), and 22 weeks after surgery prior to explantation (c). Additionally, samples from the tibia were collected to confirm histologically the osseointegration at 22 weeks of implant placement (a and b). Photomicrograph (d) shows a panoramic view of the implant and the peri-implant bone, and (e) shows in detail the bone implant contact and the newly-formed bone between the implant threads.

suggests fully-differentiated fibroblasts or osteoblasts (Figure 5b). In addition, analysis by EDX confirms the presence of organic remnants together with the inorganic bone constituents (calcium and phosphate) closely bound to the implant surface (Figure 5c).

Bone defect characterization after explantation

After explantation, bone defects were perfectly defined (Figure 6a). The cross-sections of the explant sites showed clearly the 3-dimensional geometry left by the implants (Figure 6b). It was even possible to differentiate the neck area from the threads.

The observation of the structure of the implant site after extraction by SEM showed that the 3D structure of the tibial compact bone had been preserved around the implant (Figure 6c). Moreover, it was possible to differentiate the Haversian canals (arrowheads in Figure 6d), which are orientated perpendicularly to the axis of the implant site. Volkmann's canals were also observed (arrows in Figure 6d), which run perpendicular to osteons, connecting the Haversian canals.

Cellularity of the bone at the explant site was analyzed by blue staining with MGG (Figure 6e). Note the shape of the implant thread in the right side of the microphotography. Osteocytes were observed in their lacunae (Figure 6f). Most of the lacunae were occupied by osteocytes, even when the lacunae were close to the surface of the implant that had been explanted. The morphology of these cells was normal with no signs of damages resulting from the explantation procedure.

Discussion

The field of oral implantology is advancing significantly due to the evolution of implant materials, placement protocols, and surgical techniques, allowing a significant increase in the implant success rates. However, there are still implants that are lost and therefore it is necessary to provide techniques that can explant implants in a predictable way and with no side effects for the patients. To that end, implant-specific reverse-torque devices have been developed and their success in explantation has been documented clinically in nearly 100 cases.[16]

This study, in a sheep tibia model, was carried out to gain more knowledge on the mechanisms underlying the non-traumatic implant explantation technique. Interestingly, resonance frequency analysis was first published in 1998 by Meredith et al[20] Since its initial description, this method has been widely used as a noninvasive measure of primary implant stability,[17,21] although there are some studies that do no correlate the ISQ with the value of bone-implant contact (BIC).[22,23] The ISQ data presented herein showed that the implants increase their stability after 22 weeks of osseointegration. During explantation, the ISQ values obtained after

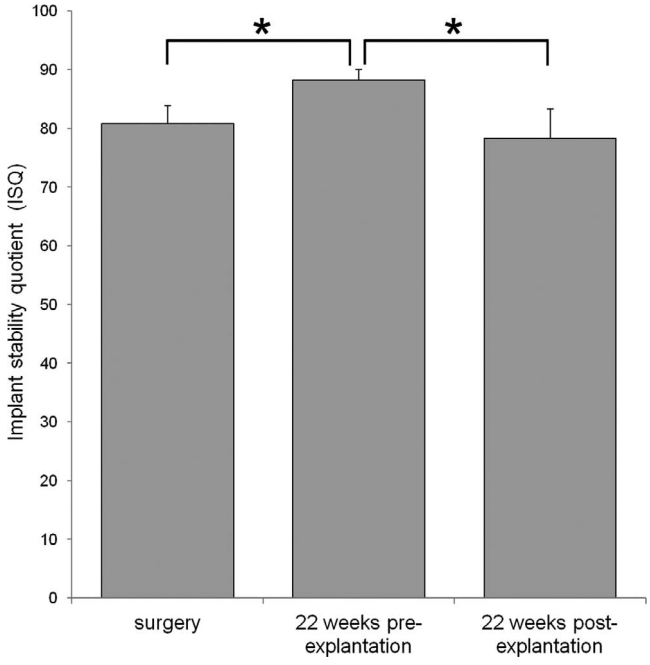

Figure 3. Resonance frequency analysis. Implant stability quotient (ISQ) was measured at the day of implantation, 22 weeks postimplantation, before and after osseointegration breakage. *Statistically significant differences ($P < 0.05$).

reaching the maximum removal torque confirm the return to the values of the primary stability obtained at the day of implantation.

Removal torque was first associated to osseointegration and bone-implant values in the late '80s.[24] Here, we have measured the removal torque values and complemented this information with the corresponding angular displacement. The angular displacement allows evaluating the extension of the process of breakage of the osseointegration. This process begins already in the first region of the curve shown in Figure 4c because this region is not fully linear, which would correspond to a pure elastic behavior, and intensifies in the next region until the final breakage at the maximum torque. The angular displacement corresponding to that torque was below 20°. After this point, only small forces are needed to overcome the remaining friction between the implant and the host bone. Additionally, the coefficient of variation for the removal torque measurements was only 7.9%, indicating that the procedure was highly reproducible. It has to be assumed, however, that differences in the cortical thicknesses and bone types will surely increase the variability with respect to the coefficients of variation obtained here.[25,26] In the clinical setting, countertorque extraction of orthodontic mini-implants is a common practice, although the forces exerted in their extraction are significantly lower than those of typical dental implants.[27,28]

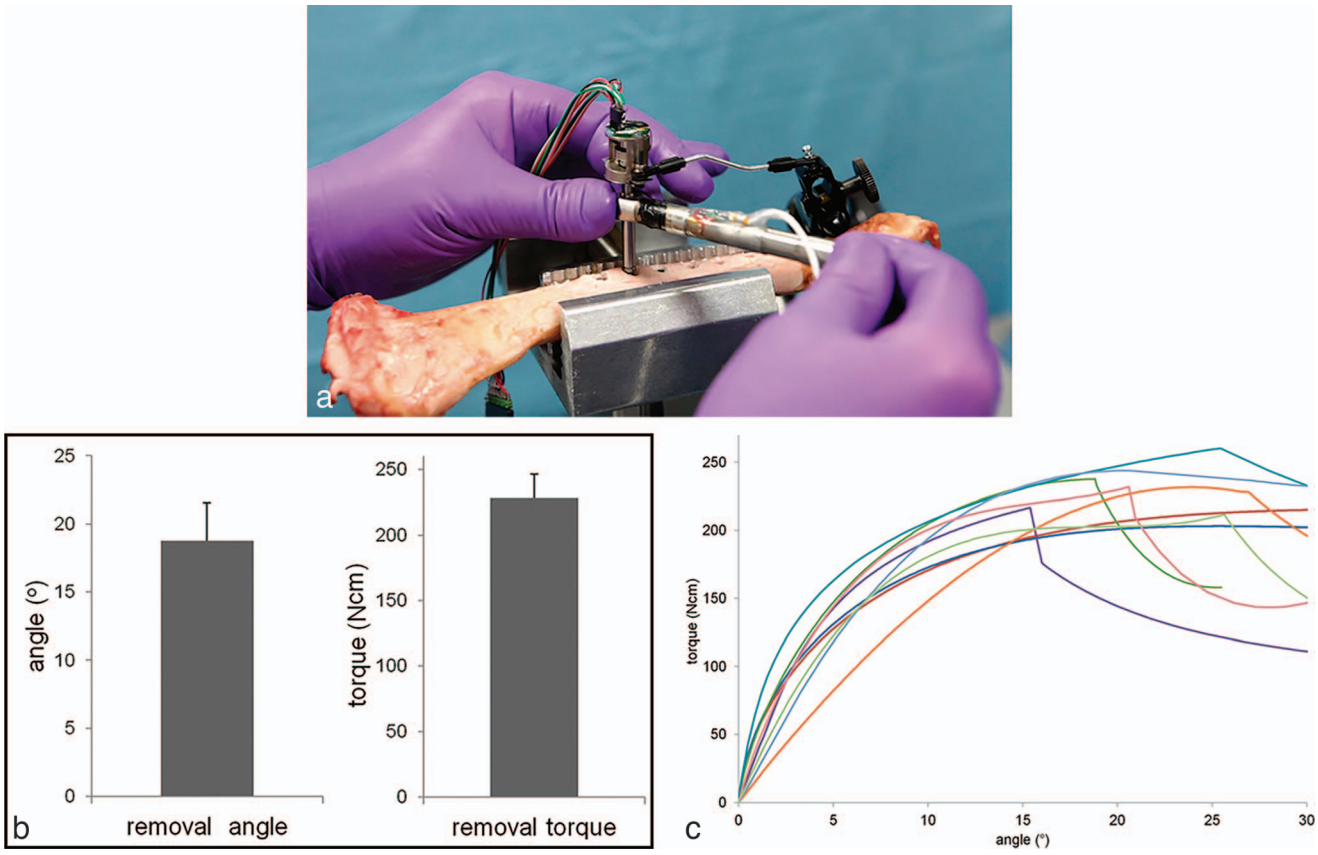

Figure 4. (a) Custom-made device for implant removal torque and angular displacement measurement. (b) Average removal angle corresponding to the maximum removal torque during explantation (data are expressed as mean + *SD*). (c) Removal torque vs angular displacement curves of 9 explantations. The experimental points have been linked together for better viewing.

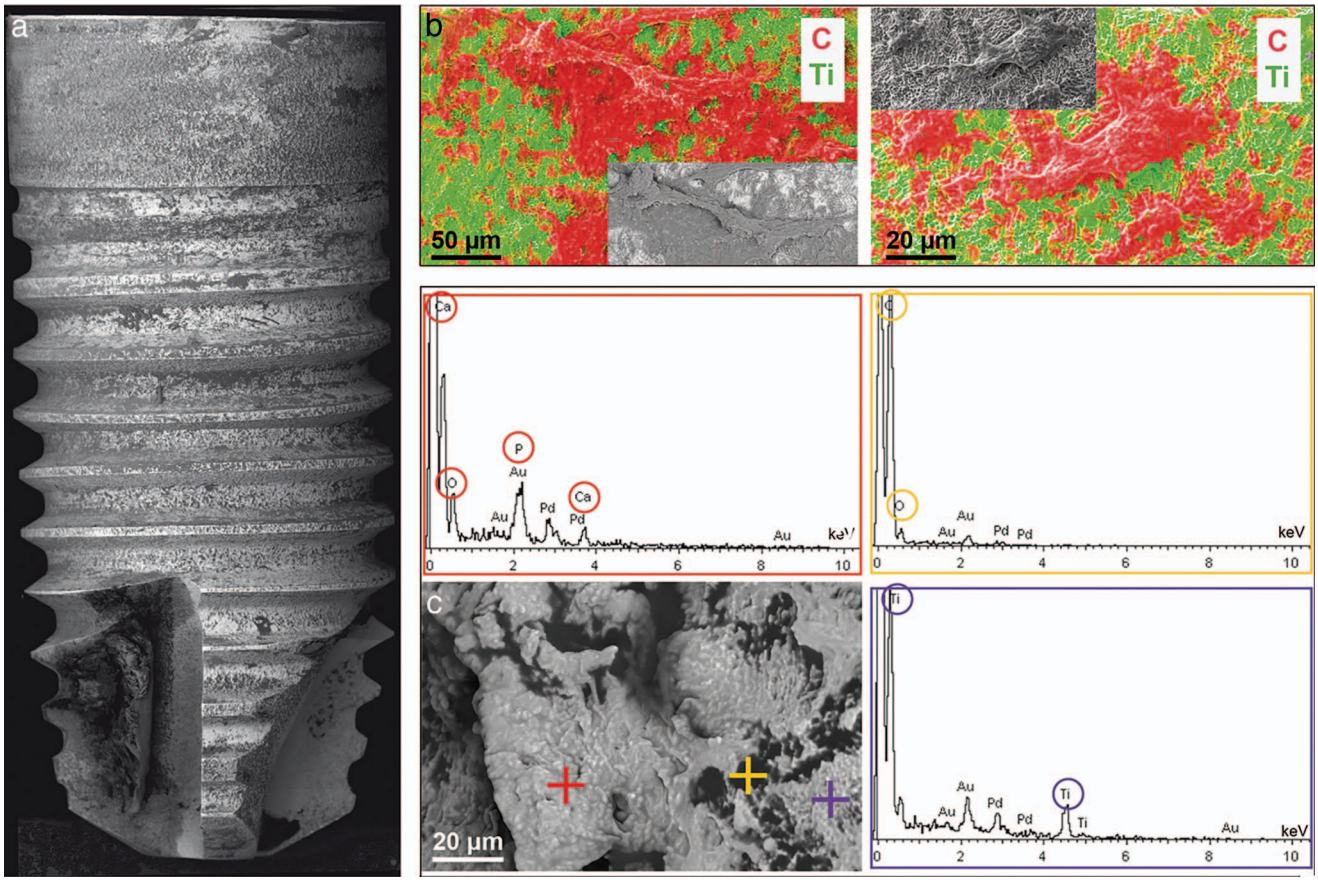

Figure 5. (a) Scanning electron micrographs showing the surface state of an implant after explantation. Only the apical region accumulates macroscopic remnants of bone. (b) EDX mapping of carbon (red) and titanium (green) on scanning electron micrographs taken at the implant neck after explantation. Cells on the surface present spread morphology, which is characteristic of attachment and differentiation. (c) Close-up scanning electron micrograph on the surface showing the bare implant surface: purple EDX spectrum at the purple cross, organic remnants: yellow EDX spectrum at the yellow cross and calcium phosphate remnants of bone: red EDX spectra at the red cross.

After explantation, the implant surface remains covered by a thin organic/inorganic layer. The fact that small bone remnants were found closely bound to the surface, suggests that at least part of the breakage of the osseointegration occurs at the bone–bone interface rather than at the bone–implant interface. The presence of osteoblasts in close contact with the implant surface has already been described, as a part of the bone modeling and remodeling processes.[29–31] However, although some bone may be observed attached to the implant during the explantation process, both the basic structure of bone and the cellularity are maintained at the explant site. These findings are particularly relevant as the presence of both viable osteocytes and a virtually intact 3D-supporting structure (native bone) can facilitate new implant osseointegration, even in the same surgical procedure. This new explantation protocol preserves almost all the bone surrounding the implant bed and the integrity of the walls. The latter will facilitate the regeneration of the defect, the installation of a new implant, or the modification of the angulation in case the implant is located very vestibular.

In addition, since the bone bed is not damaged, implant osseointegration may be accelerated with respect to the classical trephination method, regardless of the surgical steps needed. Unlike the results of Ivanoff et al,[32] fracture lines radiating from implant threads were not observed in the bone samples. This absence may be due to the sample processing method, or to the different characteristics of the implant surface, the host bone, or the insertion protocol used.

It could be argued that the bone structure of the animal model used in this study differs from that of the upper and lower human jawbone.[33] Nevertheless, these results can be extrapolated in terms of bone quality preservation considering that lower torques (below 150 Ncm) are generally required to achieve explantation in humans.[16]

Conclusions

This animal study investigates the insights of an implant extraction approach in a sheep tibiae model. Results show that minimally aggressive and predictable implant explantation can be achieved using this nontraumatic implant explantation approach. This technique causes minimal damage to the surrounding bone structure and maintains cell viability. As a result, this approach allows the substitution of failed implants even in a single surgical act and emerges as a promising strategy to resolve some clinically challenging situations.

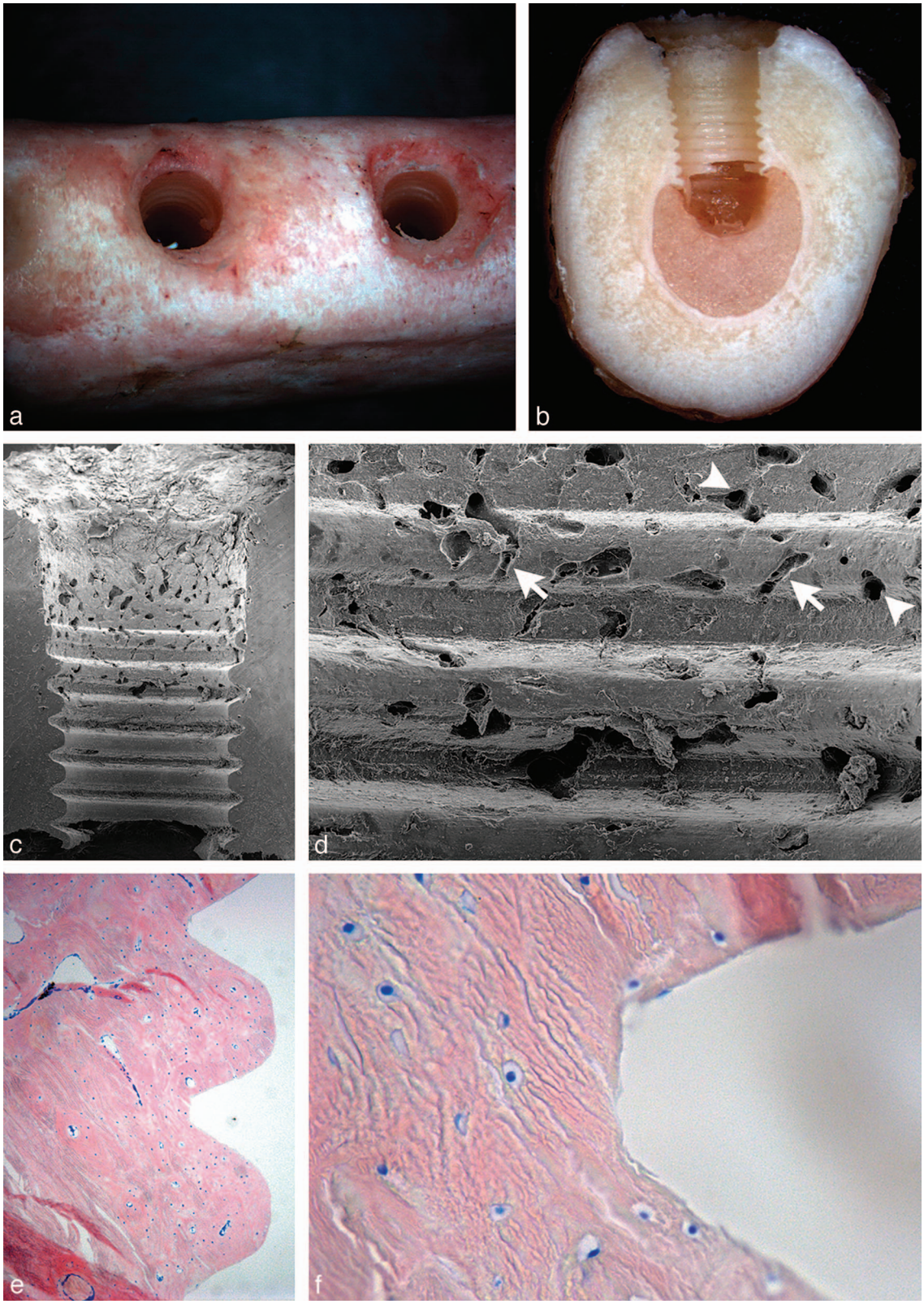

Figure 6. Characterization of the bone at explant sites. (a) Image of 2 implant sites after explantation. (b) Cross-section of the tibia showing the bone bed. Note the marks left by both the neck and the threads of the implant. (c) SEM micrograph showing the structure of the bone at the explant site. (d) At higher magnifications, both the Haversian canals (arrowheads) and the Volkmann canals (arrows) can be distinguished. (e, f) Optical micrographs showing the cellularity at the explant site (MGG staining). Viable osteocytes were observed within lacunae (blue staining).

Acknowledgment

Eduardo Anitua is the scientific director of, and Roberto Prado and Ricardo Tejero are scientists at BTI-Biotechnology Institute, the company that has developed a nontraumatic implant explantation system.

References

1. Albrektsson T, Donos N, Working G. Implant survival and complications. The Third EAO consensus conference 2012. *Clin Oral Implants Res*. 2012;23(Suppl 6):63–65.

2. Del Fabbro M, Testori T, Francetti L, Taschieri S, Weinstein R. Systematic review of survival rates for immediately loaded dental implants. *Int J Periodontics Restorative Dent*. 2006;26:249–263.

3. Anitua E, Orive G, Aguirre JJ, Ardanza B, Andia I. 5-year clinical experience with BTI dental implants: risk factors for implant failure. *J Clin Periodontol*. 2008;35:724–732.

4. Albrektsson TO, Johansson CB, Sennerby L. Biological aspects of implant dentistry: osseointegration. *Periodontol 2000*. 1994;4:58–73.

5. Branemark PI, Hansson BO, Adell R, et al. Osseointegrated implants in the treatment of the edentulous jaw. Experience from a 10-year period. *Scand J Plast Reconstr Surg Suppl*. 1977;16:1–132.

6. Sakka S, Coulthard P. Implant failure: etiology and complications. *Med Oral Patol Oral Cir Bucal*. 2011;16:e42–e44.

7. Misch CE, Perel ML, Wang HL, et al. Implant success, survival, and failure: the International Congress of Oral Implantologists (ICOI) Pisa Consensus Conference. *Implant Dent*. 2008;17:5–15.

8. Montes CC, Pereira FA, Thome G, et al. Failing factors associated with osseointegrated dental implant loss. *Implant Dent*. 2007;16:404–412.

9. Sakka S, Baroudi K, Nassani MZ. Factors associated with early and late failure of dental implants. *J Investig Clin Dent*. 2012;3:258–261.

10. Dvorak G, Franz A, Pommer B, Tangl S, Cvikl B. Explantation techniques for fractured dental implants. *J Stomat Occ Med*. 2012;5:143–146.

11. Smith LP, Rose T. Laser explantation of a failing endosseous dental implant. *Aust Dent J*. 2010;55:219–222.

12. Froum S, Yamanaka T, Cho SC, Kelly R, St James S, Elian N. Techniques to remove a failed integrated implant. *Compend Contin Educ Dent*. 2011;32:22–30.

13. Massei G, Szmukler-Moncler S. Thermo-explantation. A novel approach to remove osseointegrated implants. *Eur Cell Mater*. 2004;7 (Suppl 2):48.

14. Beolchini M, Lilliu S, Faria P, Botticelli D. Implant removal by means of an expansion of the alveolar bony crest: report of a clinical technique. *Oral Surg*. 2012;5:59–63.

15. Barclay C, Cunliffe J. Removal of a dental implant: An unusual case report. *J Dent Implant*. 2011;1:22–25.

16. Anitua E, Orive G. A new approach for atraumatic implant explantation and immediate implant installation. *Oral Surg Oral Med Oral Pathol Oral Radiol*. 2012;113:e19–e25.

17. Mathieu V, Vayron R, Richard G, et al. Biomechanical determinants of the stability of dental implants: influence of the bone-implant interface properties. *Journal of Biomechanics*. 2014;47:3–13.

18. Anitua E, Carda C, Andia I. A novel drilling procedure and subsequent bone autograft preparation: a technical note. *Int J Oral Maxillofac Implants*. 2007;22:138–145.

19. Yang R, Davies CM, Archer CW, Richards RG. Immunohistochemistry of matrix markers in Technovit 9100 New-embedded undecalcified bone sections. *Eur Cell Mater*. 2003;6:57–71.

20. Meredith N. Assessment of implant stability as a prognostic determinant. *Int J Prosthodont*. 1998;11:491–501.

21. von Wilmowsky C, Moest T, Nkenke E, Stelzle F, Schlegel KA. Implants in bone: Part II. Research on implant osseointegration: material testing, mechanical testing, imaging and histoanalytical methods. *Oral Maxillofac Surg*. 2014;18:355–372.

22. Nkenke E, Hahn M, Weinzierl K, Radespiel-Troger M, Neukam FW, Engelke K. Implant stability and histomorphometry: a correlation study in human cadavers using stepped cylinder implants. *Clin Oral Implants Res*. 2003;14:601–609.

23. Huang HL, Tsai MT, Su KC, et al. Relation between initial implant stability quotient and bone-implant contact percentage: an in vitro model study. *Oral Surg Oral Med Oral Pathol Oral Radiol*. 2013;116:e356–e361.

24. Johansson C, Albrektsson T. Integration of screw implants in the rabbit: a 1-year follow-up of removal torque of titanium implants. *Int J Oral Maxillofac Implants*. 1987;2:69–75.

25. Miyamoto I, Tsuboi Y, Wada E, Suwa H, Iizuka T. Influence of cortical bone thickness and implant length on implant stability at the time of surgery–clinical, prospective, biomechanical, and imaging study. *Bone*. 2005; 37:776–780.

26. Pithon MM, Nojima MG, Nojima LI. In vitro evaluation of insertion and removal torques of orthodontic mini-implants. *Int J Oral Maxillofac Surg*. 2011;40:80–85.

27. Kim SH, Cho JH, Chung KR, Kook YA, Nelson G. Removal torque values of surface-treated mini-implants after loading. *Am J Orthod Dentofacial Orthop*. 2008;134:36–43.

28. Okazaki J, Komasa Y, Sakai D, et al. A torque removal study on the primary stability of orthodontic titanium screw mini-implants in the cortical bone of dog femurs. *Int J Oral Maxillofac Surg*. 2008;37:647–650.

29. Morinaga K, Kido H, Sato A, Watazu A, Matsuura M. Chronological changes in the ultrastructure of titanium-bone interfaces: analysis by light microscopy, transmission electron microscopy, and micro-computed tomography. *Clin Implant Dent Relat Res*. 2009;11:59–68.

30. Okamatsu K, Kido H, Sato A, Watazu A, Matsuura M. Ultrastructure of the interface between titanium and surrounding tissue in rat tibiae–a comparison study on titanium-coated and -uncoated plastic implants. *Clin Implant Dent Relat Res*. 2007;9:100–111.

31. Murai K, Takeshita F, Ayukawa Y, Kiyoshima T, Suetsugu T, Tanaka T. Light and electron microscopic studies of bone-titanium interface in the tibiae of young and mature rats. *J Biomed Mater Res*. 1996;30:523–533.

32. Ivanoff CJ, Sennerby L, Johansson C, Rangert B, Lekholm U. Influence of implant diameters on the integration of screw implants. An experimental study in rabbits. *Int J Oral Maxillofac Surg*. 1997;26:141–148.

33. Pearce AI, Richards RG, Milz S, Schneider E, Pearce SG. Animal models for implant biomaterial research in bone: a review. *Eur Cell Mater*. 2007;13:1–10.